

# **Cross-Field Blob Transport in Tokamak Scrape-off Layer Plasmas**

**D. A. D'Ippolito and J. R. Myra**

*Lodestar Research Corporation, 2400 Central Avenue, Boulder, Colorado 80301*

**S. I. Krasheninnikov**

*University of California, San Diego, California*

July 12, 2001; revised August 31, 2001

(submitted to Physics of Plasmas)

---

DOE/ER/54392-10

LRC-01-83

---

**LODESTAR RESEARCH CORPORATION**

# Cross-Field Blob Transport in Tokamak Scrape-off Layer Plasmas\*

**D. A. D'Ippolito<sup>†</sup> and J. R. Myra**

*Lodestar Research Corporation, 2400 Central Avenue, Boulder, Colorado 80301*

**S. I. Krasheninnikov**

*University of California, San Diego, California*

## **Abstract**

Recent measurements show that non-diffusive, intermittent transport of particles can play a major role in the scrape-off-layer (SOL) of fusion experiments. A possible mechanism for fast convective plasma transport is related to the plasma filaments or “blobs” observed in the SOL with fast cameras and probes. In this paper, physical arguments suggesting the importance of blob transport [S. I. Krasheninnikov, *Physics Letters A* **283**, 368 (2001)] have been extended by calculations using a three-field fluid model, treating the blobs as coherent propagating structures. The properties of density, temperature and vorticity blobs, and methods of averaging over ensembles of blobs to get the average SOL profiles, are illustrated. The role of ionization of background neutrals in sustaining the density blob transport is also discussed. Many qualitative features of the experiments, such as relatively flat density profiles and transport coefficients increasing toward the wall, are shown to emerge naturally from the blob transport paradigm.

PACS numbers: 52.25.Fi, 52.35.Ra, 52.55.Dy, 52.55.Fa

†email: [dasd@lodestar.com](mailto:dasd@lodestar.com)

## I. Introduction

Recently a new picture of transport in the edge and scrape-off-layer (SOL) region has begun to emerge from experiments and theory, which has the following elements:

(1) Experimental data from tokamaks<sup>1-5</sup> and other plasma devices<sup>6</sup> suggests that radial transport in the SOL has a two-scale structure: the measured SOL density profiles have an exponential decay near the last closed flux surface (LCFS) followed by an outer “shoulder” region in which the profile is relatively flat. The effective diffusion coefficient inferred from these profiles increases towards the wall, suggesting that the transport is primarily convective in the “far SOL” away from the LCFS. In several tokamaks, this convective transport is rapid enough that the particle fueling is dominated by recycling from the wall, rather than from the divertor, implying that the idealized picture of divertor operation may need to be modified.<sup>2</sup>

(2) The SOL density and particle flux tend to be *intermittent* in space and in time. This behavior is seen in nonlinear turbulence codes (e.g. see Refs. 7-9) and in experiments<sup>10-16</sup> using probes and turbulence imaging diagnostics.

(3) Turbulence simulation codes<sup>7-9</sup> and diagnostics<sup>10-16</sup> show the existence of coherent structures (“radial streamers”, “filaments” and “blobs”) in the edge and SOL plasmas in the strongly turbulent regime. These structures are more localized perpendicular to the magnetic field  $\mathbf{B}$  than along it, and sometimes involve radial propagation and transport of particles across the field.

It has been suggested<sup>17</sup> that these three properties are all related, viz. that the rapid, intermittent convection of particles can be explained by the turbulent formation and radial propagation of high density plasma blobs. The basic idea is the following. Consider a coherent structure with a higher density than the surrounding plasma, which is localized in the radial-poloidal plane perpendicular to  $\mathbf{B}$  but is extended along the field lines. From the three-dimensional point of view, this structure looks like a filament; indeed, glowing

filaments have been observed in the SOL of Spherical Torus experiments.<sup>14,15</sup> In the two-dimensional cross-section normal to  $\mathbf{B}$ , these structures look like “blobs” of excess density, and we will adopt this terminology in the present paper. In the presence of a charge-dependent drift (e.g. induced by the curvature or centrifugal force), the blob becomes polarized and an electric field forms due to the effective “sheath resistivity”.<sup>18</sup> The resulting  $\mathbf{E} \times \mathbf{B}$  drift moves the blobs to the outer wall.

In the present paper, we extend the physical arguments of Ref. 17 by calculations using a three-field (density, temperature, potential) Braginskii fluid model. Here, we ignore the turbulent origin of the blobs and treat them simply as coherent propagating structures. Moreover, for most of the paper we limit the discussion to the far SOL region in which the diffusive background density is negligible and treat the blobs as isolated and non-interacting. In this model the local density, temperature and vorticity are intermittent in space and time, and radial transport is inherently convective. The existence of relatively flat density profiles extending to the wall, and effective transport coefficients increasing toward the wall, emerge naturally from the blob transport paradigm, independent of the details of the blob creation. Finally, if the blobs reach the wall before decaying, the resulting SOL equilibrium depends on wall recycling and ionization, and there is a minimum plasma flux required to sustain the equilibrium. All of these features of the model are in qualitative agreement with experiments.

The plan of this paper is the following. In Sec. II we describe the approximations and equations in the model. In Sec. III, the properties of single blobs of density, temperature and vorticity are elucidated, the validity conditions of the model are examined, and the physical picture of blob transport is summarized. In Sec. IV, we discuss methods of averaging over the size distribution of an ensemble of blobs to get the average SOL profiles. The role of ionization of background neutrals in sustaining the density blob transport is discussed in Sec. V. A summary and discussion of the blob model is given in Sec. VI. Appendix A discusses the generalization of the blob model to

include a sheared flow  $u_y(x)$ . Appendix B gives an analytic criterion for the boundary between the large and small-blob transport regimes for the special case of a power-law distribution of blob radii.

## II. The Model

As described in the previous section, the physical picture emerging from many experiments is that the SOL has two regions. The first region, located within one exponential density decay length of the LCFS has the following properties: the density profile is determined by balancing radial diffusion from the core with parallel particle losses to the sheaths, neutral particle effects are usually not dominant, and the X-point (if there is a separatrix) can give significant variation along  $\mathbf{B}$ . The blobs are created in this region, probably by turbulent processes or avalanches<sup>19,20</sup>. The creation process is not yet understood and is outside the scope of the present paper. In the second region (the far SOL), we assume that the profiles are dominated by blob convection, so that the detailed transport of particles, energy and vorticity is intermittent in space and in time. Neutrals can be important in this outer region, and the profile shape depends on both the blob distribution and on neutral ionization, which can sustain the blob transport. In this outer region, spatial variation parallel to  $\mathbf{B}$  will be neglected. The model described in this section applies mainly in the outer SOL region.

We employ a simple set of equations that allows a solution for SOL blobs with local concentrations of density, temperature or vorticity. The model consists of the following vorticity, continuity and temperature equations:

$$\frac{c^2}{B^2} nm_i \frac{d}{dt} \nabla_{\perp}^2 \Phi = \nabla_{\parallel} J_{\parallel} + \frac{2c}{B} \mathbf{b} \times \boldsymbol{\kappa} \cdot \nabla p \quad , \quad (1)$$

$$\frac{dn}{dt} + \nabla_{\parallel} (nu_{\parallel}) = \xi n \quad , \quad (2)$$

$$\frac{dT_e}{dt} + \nabla_{\parallel} (u_{\parallel} T_e) = \frac{2}{3n} \nabla_{\parallel} \kappa_{\parallel} \nabla_{\parallel} T_e - \xi E_i \quad , \quad (3)$$

where  $d/dt = \partial/\partial t + \mathbf{v}_E \cdot \nabla$ ,  $\mathbf{v}_E = (c/B) \mathbf{b} \times \nabla_{\perp} \Phi$ ,  $\mathbf{B} = B\mathbf{b}$  is the magnetic field,  $\kappa = \mathbf{b} \cdot \nabla \mathbf{b}$  is the magnetic curvature,  $J_{\parallel}$  is the current density and  $u_{\parallel}$  is the mass flow velocity parallel to  $\mathbf{B}$ ,  $n = n_e = n_i$  is the particle density,  $p = n(T_e + T_i)$  and  $p_e = nT_e$  are the total and electron pressures, respectively,  $\kappa_{\parallel}$  is the parallel heat conductivity,  $\xi = n_0 \langle \sigma v \rangle_i$  is the neutral particle ionization rate and  $n_0$  is the neutral density, and  $(3/2)E_i$  is the total energy cost per ionization (including losses from non-ionizing collisions and the energy cost of heating the ionized electron to the temperature  $T_e$ ). All other symbols have their usual meanings. The derivation of the curvature term in Eq. (1) uses the approximation  $\mathbf{J} \cdot \nabla p = 0$ , which implies  $\mathbf{b} \cdot \nabla p \times \nabla(\ln B) = \mathbf{b} \cdot \nabla p \times \kappa$ , so that the factor of 2 in Eq. (1) accounts for both the  $\nabla B$  and curvature drifts. We assume  $T_e \gg T_i$  for simplicity and have neglected a number of small terms on the right-hand sides (rhs) of Eqs. (2) and (3) that are higher order in the small parameters defined subsequently. None of these assumptions is essential, but they simplify the presentation. For typical parameters, the parallel heat diffusion term  $\propto \kappa_{\parallel}$  dominates the temperature equation and forces  $T_e$  to be nearly constant along the field lines.

These equations can be simplified by integrating along the field lines in the limit where all quantities are assumed to be constant along  $\mathbf{B}$ . The terms involving parallel derivatives are evaluated using the boundary conditions (BCs) that  $|v_{\parallel}| = c_s$  at the sheath entrance and that  $J_{\parallel}$  is matched to the sheath current:

$$J_{\parallel} = J_{\parallel \text{sh}} \equiv -\mathbf{n} \cdot \mathbf{b} n e \left( v_{\parallel} - \frac{v_e}{\sqrt{2\pi}} \exp\left(-\frac{e\Phi}{T_e}\right) \right) \quad , \quad (4)$$

where  $c_s = (T_e/m_i)^{1/2}$  is the sound speed and  $v_e = (T_e/m_e)^{1/2}$  is the electron thermal speed. Each field line is assumed to terminate at each end in grounded conducting plates

(no bias potential), and  $\mathbf{n}$  is defined to be the unit vector normal to the conducting plate and pointing into the plasma.

Carrying out the integration along the field line and converting to dimensionless form, the model equations become

$$\begin{aligned} n \frac{d}{dt} \nabla_{\perp}^2 \Phi &= \alpha n T^{1/2} \left[ 1 - \nu e^{-\Phi/T} \right] + 2 \mathbf{b} \times \boldsymbol{\kappa} \cdot \nabla p , \\ &= \alpha n T^{1/2} \left[ 1 - e^{-\phi/T} \right] + 2 \mathbf{b} \times \boldsymbol{\kappa} \cdot \nabla p , \end{aligned} \quad (5)$$

$$\frac{dn}{dt} + (\alpha T^{1/2} - \xi) n = 0 , \quad (6)$$

$$\frac{dT}{dt} + \alpha_T T^{3/2} + \xi E_i = 0 , \quad (7)$$

where  $d/dt = \partial/\partial t + \mathbf{b} \times \nabla_{\perp} \Phi \cdot \nabla$ ,  $\nu = (m_i/2\pi m_e)^{1/2}$ ,  $\alpha = 2\rho_s/L_{\parallel}$ ,  $\alpha_T = \alpha S_E$ , and  $S_E$  is the sheath energy transmission coefficient. The parameter  $\alpha$  measures the net parallel current into the plates,  $\alpha_T$  specifies the energy loss due to parallel flow to the plates, and the term  $\xi E_i$  represents the ionization energy cost. For most of the discussion, we will neglect the ionization term and treat  $\alpha$  and  $\alpha_T$  as constants. In the second form of the vorticity equation, the rhs was rewritten using the substitution

$$\Phi = \Phi_B + \varphi , \quad (8)$$

where the Bohm potential is defined by  $\Phi_B \equiv T \ln \nu \approx 3T$ . In the limit where one-dimensional sheath physics dominates Eq. (5), the potential is given by  $\Phi = \Phi_B$ , so that  $\varphi$  represents the contribution of two-dimensional physics (convection, turbulence) to the potential.

In these equations, we have normalized times to  $\Omega_i^{-1}$ , length scales to  $\rho_s$ , and other quantities to reference values (e.g. separatrix values  $n_s$  and  $T_{es}$ ). Specifically, we let  $\Omega_i dt \rightarrow dt$ ,  $\xi/\Omega_i \rightarrow \xi$ ,  $\rho_s \nabla \rightarrow \nabla$ ,  $\rho_s \boldsymbol{\kappa} \rightarrow \boldsymbol{\kappa}$ ,  $e\Phi/T_{es} \rightarrow \Phi$ ,  $v/c_s \rightarrow v$ ,  $n/n_s \rightarrow n$ ,  $T_e/T_{es}$

$\rightarrow T$ ,  $E_i/T_{es} \rightarrow E_i$ ,  $p/(n_s T_{es}) \rightarrow p$ , and  $J/(n_s e c_s) \rightarrow J$ , where  $\Omega_i = eB/m_i c$  is the ion cyclotron frequency and  $\rho_s = c_s/\Omega_i$  is the (constant) gyroradius based on  $c_s = (T_{es}/m_i)^{1/2}$ .

Since the plasma filaments are assumed to be localized perpendicular to the magnetic field, we can use a slab model with orthogonal coordinates  $\{x, y, z\}$  such that the  $x$  coordinate is taken in the direction of the major radius and the  $z$  coordinate is taken along the magnetic field. For the remainder of this paper, the coordinates are assumed to be dimensionless, normalized to  $\rho_s$ . The dimensionless curvature can be written as  $\boldsymbol{\kappa} = -(\rho_s/R) \hat{\mathbf{e}}_x$  and  $2\mathbf{b} \times \boldsymbol{\kappa} \cdot \nabla = -\beta \nabla_y$ , where  $\beta = 2\rho_s/R$  is the parameter measuring the strength of the curvature drift. We let  $x > 0$  correspond to the SOL, so that motion in the positive  $x$  direction is outwards towards the wall.

Finally, it is convenient to transform into the moving frame of the blob. This transformation is given by  $d/dt \rightarrow \partial/\partial t + \mathbf{b} \times \nabla_{\perp} \Phi \cdot \nabla - \mathbf{u} \cdot \nabla$ , where  $\mathbf{u}$  is the constant velocity of the blob in the lab frame to be determined subsequently by the solution of the equations.

Collecting all of these results, we obtain the final form of Eq. (5):

$$\frac{d}{dt} \nabla_{\perp}^2 \Phi = \alpha T^{1/2} \left[ 1 - e^{-\varphi/T} \right] - \frac{\beta}{n} \nabla_y (n T) \quad , \quad (9)$$

$$\frac{d}{dt} = \frac{\partial}{\partial t} + (\nabla_x \Phi - u_y) \nabla_y - (\nabla_y \Phi + u_x) \nabla_x \quad . \quad (10)$$

To summarize this section, the fundamental equations of our blob model are Eqs. (6)-(10). The small parameters in this problem are  $\alpha \sim \beta \sim \rho_s/R$ , and  $\nabla_{\perp} \sim \rho_s/r_b$ , where  $\rho_s$  is the gyroradius,  $R$  is the major radius of the tokamak, and  $r_b$  is a typical blob radius. In the next section, we carry out a solution of these equations by expanding in the small parameters.

### III. Single Blob Properties

We first consider the properties of isolated blobs, starting with the simple physics of particle transport and then generalizing to obtain a unified picture of density, temperature and vorticity blobs.

#### A. Density Blobs

First, we consider the case where the vorticity term on the lhs of Eq. (9) is negligible. The localized solutions of Eqs. (6), (9) and (10) can be interpreted as propagating blobs of enhanced density. To make the analysis as transparent as possible, we assume here that  $T$  is constant in time and space ( $T \rightarrow 1$ ) and expand the sheath term in Eq. (9) in the limit  $\phi \ll 1$ . The resulting equations are:

$$\alpha \phi - \frac{\beta}{n} \nabla_y n = 0 \quad , \quad (11)$$

$$\frac{dn}{dt} + (\alpha - \xi)n = 0 \quad . \quad (12)$$

with  $d/dt$  given by Eq. (10).

#### 1. Solution in Cartesian Coordinates

First, we consider the problem in the local SOL coordinates, assuming a separable solution of the form

$$n(x, y, t) = f(x)g(y)e^{-\gamma t} \quad , \quad (13)$$

where  $\gamma = \alpha - \xi$ . With this ansatz, Eqs. (11) and (12) reduce to

$$\phi = \frac{\beta}{\alpha} \frac{g'(y)}{g} \quad , \quad (14)$$

$$(\nabla_x \Phi - u_y) \nabla_y n - (\nabla_y \Phi + u_x) \nabla_x n = 0 \quad . \quad (15)$$

Since Eq. (14) implies  $\nabla_x \phi = 0$ , the solution of Eq. (15) yields  $u_x = -\nabla_y \Phi$  and  $u_y = \nabla_x \Phi_B = 0$  for constant temperature. With  $\phi$  given by Eq. (14), we have that  $(\beta/\alpha) (g'/g)' =$

$-u_x$ , which is constant in our frame transformation. Integrating gives a Gaussian solution,  $g(y) = n_b \exp[-(y^2/2y_b^2)]$ , and we find that

$$u_x = \frac{\beta}{\alpha} \frac{1}{y_b^2}, \quad u_y = 0, \quad (16)$$

for *any*  $f(x)$ . [For the special case  $f = \text{const.}$ , one obtains a radial streamer propagating outwards in  $x$ .] Note that  $u_x$  is constant in space for constant  $y_b$ . Also note that the neglect of the vorticity term on the lhs of Eq. (9) poses no restriction on this solution which has  $\Phi \propto y$  and  $\nabla_{\perp}^2 \Phi = 0$ .

This simple solution has a number of interesting physical properties. The density blob decays on a time scale  $\tau_n = 1/\gamma = 1/(\alpha - \xi)$ , which represents a balance between particles lost by sonic flow to the plates (the  $\alpha$  term) and resupplied by ionization (the  $\xi$  term). A steady state can be obtained if the ionization is fast enough ( $\xi = \alpha$ ). A potential  $\Phi(y)$  is formed because of the curvature-drift-induced charge separation in the blob ( $\propto \beta/y_b^2$ ). This charge polarization is inhibited by the parallel loss of particles ( $\propto \alpha$ ). The associated electric field  $E_y$  gives a radial drift  $u_x$  of the blob outwards across the SOL, and the drift is faster for smaller blobs ( $u_x \propto 1/y_b^2$ ). Pushing fluid theory to the limit, we find that for blobs of order the gyroradius ( $y_b \sim 1$ ) the radial velocity is of order the sound speed ( $u_x \sim 1$ )!

## 2. Solution in Cylindrical Coordinates

A different point of view than in the previous section, which is perhaps more intuitive in the case where vorticity plays a role, is to think of a plasma filament as having approximate cylindrical symmetry about a magnetic field line. To pursue this line of thought, we introduce cylindrical blob coordinates  $(r, \theta)$  defined by  $x = r \cos \theta$ ,  $y = r \sin \theta$ . We emphasize that these coordinates are relative to the blob axis and defined in the moving blob frame; they do not refer to the magnetic axis of the torus.

One can find solutions to Eqs. (11) and (12) in this cylindrical coordinate system. Again, we neglect the vorticity term, assume constant temperature ( $T = 1$ ) and start with the ansatz

$$\begin{aligned} n(\mathbf{r}, t) &= n(r) e^{-\gamma t} , \\ \varphi(r, \theta, t) &= \varphi(r, \theta) e^{-\gamma t} , \end{aligned} \quad (17)$$

where  $\gamma = \alpha - \xi$ . Substituting this ansatz into Eqs. (11) and (12) yields

$$\varphi = \frac{\beta}{\alpha} \sin \theta \frac{\partial}{\partial r} \ln n(r) , \quad (18)$$

$$\left( \frac{1}{r} \frac{\partial \varphi}{\partial \theta} - \nabla_x \Phi_B \sin \theta + u_x \cos \theta + u_y \sin \theta \right) \frac{\partial}{\partial r} n(r) = 0 . \quad (19)$$

Combining these equations determines the drift velocity to order  $1/r_b$

$$u_x = -\frac{\beta}{\alpha} \frac{1}{r} \frac{\partial}{\partial r} \ln n(r) , \quad u_y = 0 . \quad (20)$$

Thus, we recover an analogous solution to the one given in slab coordinates, except that now the blob is confined in the  $r$  direction and has cylindrical symmetry to lowest order. For the frame transformation  $u_x = \text{const.}$ , integrating Eq. (20) gives a Gaussian density profile,  $n(r) = n_b \exp[-(r^2/2r_b^2)]$ , so that

$$u_x = \frac{\beta}{\alpha} \frac{1}{r_b^2} , \quad u_y = 0 . \quad (21)$$

The same picture holds with  $r_b$  taking the place of  $y_b$ . Again, the smallest blobs move fastest in the  $x$  direction (i.e. outwards), reaching the sound speed for  $r_b \sim 1$ . Since Eq. (18) implies  $\varphi \sim r \sin \theta$  and hence  $\nabla_{\perp}^2 \varphi = 0$ , one may in fact retain the vorticity term in Eq. (9) but it has no effect. With zero vorticity, the model equations do not set a limit on the minimum size of the density blobs, other than the condition for the validity of fluid

theory itself ( $r_b > 1$ ). As before, the density blobs can be maintained in steady-state ( $\gamma = 0$ ) by ionization.

If we assume that an ensemble of blobs of size  $r_b$  is responsible for the SOL density, one can estimate the SOL width (or radial scale length) from this model by computing the distance the blobs travel before decaying,  $L_{nx} \approx u_x \tau_n = (\beta/\alpha)/[(\alpha-\xi)r_b^2]$ . Note that the SOL density profile flattens for small blobs ( $r_b \rightarrow 0$ ) or for strong ionization ( $\xi \rightarrow \alpha$ ).

So far, we have assumed a constant temperature,  $T(x) = 1$ , and neglected any other mechanism for producing a “poloidal” velocity  $u_y$ . This solution can be extended to include a sheared  $u_y(x)$  component of the blob velocity with scale length  $L$  larger than a blob size ( $L \gg r_b$ ), as discussed in Appendix A. The sheared velocity could be produced by biasing the divertor end plates or by the effect of a radial temperature gradient,  $T = T(x)$ . In the Appendix, we show that the sheared  $u_y(x)$  can significantly distort the blob shape, but the radial velocity  $u_x$  is unaffected by general velocity shear. However, there are two effects which can slow the radial propagation of the blobs. First, when  $T(x)$  is included in the analysis, one finds that  $u_x \propto [T(x)]^{3/2}$  and  $u_y \propto -y \partial_x [T(x)]^{3/2}$ , so the radial velocity of the blob is reduced and the blob is stretched in  $y$  as it propagates down the temperature gradient in the SOL. Another effect which can reduce  $u_x$  is the averaging over the spatial variation of the curvature required for poloidally-extended blobs. These effects are mentioned here for completeness, but in the rest of the paper we restrict the discussion to the situation described in this section in which  $u_x = \text{constant}$  and  $u_y = 0$ .

Returning to the main line of argument, we have shown that density blob solutions exist with either rectangular or cylindrical symmetry. In the latter case, it would be more satisfying on physical grounds if the assumption of cylindrical symmetry were justified by strong rotation of the blob around its axis (vorticity), although it is not necessary for the mathematical consistency of the solution. In the next section, we

generalize the discussion by looking for solutions in which the vorticity is large and in which both the vorticity and temperature are time dependent.

### **B. Temperature and Vorticity Blobs**

If the blobs are formed by some turbulent process ejecting material from inside the separatrix into the SOL, it is likely that the blobs will not only have a density higher than the ambient SOL density, but also a higher temperature and vorticity as well. To describe this situation, we solve the full set of Eqs. (6)-(10). In this section, we will focus the discussion on spatial variation of the density and vorticity on the scale of the blob size  $r_b$  and neglect spatial variation on the longer scale length of the SOL profiles.

There are two contributions to the electrostatic potential [see Eq. (8)]. As a result of the sheath BCs in the SOL, there is the Bohm sheath potential  $\Phi_B \approx 3T$ , which arises to confine the electrons streaming along the field lines and to ensure quasineutrality of the SOL plasma. If the blob has a higher temperature than its surroundings,  $\Phi_B(r)$  will be a decreasing function of the blob radius and will generate vorticity. Thus, blob temperature is one possible mechanism of symmetrizing the blob. Other sources of vorticity in the initial blob formation process are represented in Eq. (8) by the potential  $\varphi$ . We will show that these two contributions to the vorticity decay in time by different physical effects.

We restrict the present analysis to the case of cylindrically-symmetric density, temperature and potentials, so that the convective terms in  $d/dt$  vanish. To permit an analytic solution for the time dependence of these fields, we treat  $T(r) = T_0$  as spatially constant in the blob (so that the blob size is determined by the density profile) and neglect the effect of ionization.

Assuming separable solutions in  $r$  and  $t$ , one can then integrate Eqs. (6) and (7) in time to obtain the following results:

$$n(r, t) = \frac{n(r)}{\left(1 + \frac{t}{\tau_T}\right)^{\frac{2\alpha}{\alpha_T}}}, \quad T(t) = \frac{T_0}{\left(1 + \frac{t}{\tau_T}\right)^2}, \quad (22)$$

where  $\alpha_T = \alpha S_E$  and  $\tau_T = 2/(\alpha_T T_0^{1/2})$  is the temperature decay time. Here  $T_0$  denotes the temperature of the blob as it detaches from the LCFS at  $t = 0$ . Note that the blob density and temperature do not decay exponentially in time, but decay by power laws because of the  $T$  dependence of the parallel loss terms in Eqs. (6) and (7). Since the density exponent  $2\alpha/\alpha_T = 2/S_E \ll 1$  is typically much smaller than the temperature exponent, the temperature decays more rapidly than the density. It is straightforward to show that the density decays exponentially [ $\propto \exp(-\alpha T_0^{1/2} t)$ ] in the limit where  $T$  is independent of time ( $\alpha_T \rightarrow 0$ ). This limit with  $T_0 = 1$  was considered in Sec. III A and yields the density decay time  $\gamma_n = \alpha$  in the absence of ionization.

The potential in the blob has the form

$$\Phi(r, t) = \Phi_B(t) + \varphi_0(r) e^{-\gamma_\varphi t}, \quad (23)$$

where  $\Phi_B = 3 T_0(t)$ . The potential  $\varphi_0(r)$  in Eq. (23), which is of order  $(1/r_b)^0$ , should not be confused with the potential  $\varphi(r, \theta)$  in the previous section, which is of order  $(1/r_b)$ . The two potentials represent different physical processes acting on different time scales, as will become apparent. The Bohm sheath potential  $\Phi_B$  decays on the temperature time scale  $\tau_T$ , which is much shorter than the density time scale  $\tau_n \approx \tau_T \alpha_T / \alpha \approx 1/\alpha$  because the parallel energy transport is much faster than the particle transport. This suggests that it is physically self-consistent to assume that the blob rotation due to  $E_r = -\nabla_r \Phi_B(r)$  symmetrizes the blob density [ $n(r, \theta) \rightarrow n(r)$ ] on the fast time scale  $\tau_T$ , although this effect has not been included in our analytic solution.

The decay rate  $\gamma_\varphi$  of the remaining contribution to the potential can be calculated as follows. We consider the limit in which  $\varphi_0$  decays in time much faster than  $T$ , so that the temperature can be treated as a constant, which we set to unity. The validity condition

for neglecting the time dependence of  $T$  is  $\alpha r_b^2 \gg \alpha_T$ , as can be verified *a posteriori*, which implies  $r_b^2 \gg S_E$ . In this limit and using the assumption of cylindrical symmetry, the lowest order part of Eq. (9) [neglecting the small terms proportional to  $\beta$ ] reduces to

$$\frac{\partial}{\partial t} \nabla_{\perp}^2 \varphi = \alpha \left[ 1 - e^{-\varphi} \right] , \quad (24)$$

where to simplify the notation we have suppressed the subscript on  $\varphi_0$ . If  $\varphi$  is large, the exponential term in Eq. (24) can be neglected and this equation yields a linear decay of  $\varphi$  with time. When the potential decays to the level that  $\varphi \ll 1$ , one can expand the exponential factor so that the rhs of Eq. (24) equals  $\alpha\varphi$ . Defining  $k^2 = \alpha/\gamma_{\varphi}$  one can put this equation in the form of a Bessel's equation:

$$\frac{1}{r} \frac{\partial}{\partial r} r \frac{\partial}{\partial r} \varphi + k^2 \varphi = 0 . \quad (25)$$

A particular solution to this equation is  $\varphi \sim J_0(kr)$ ; therefore, the general solution for  $\varphi$  is given by

$$\varphi(r, t) = \int_0^{\infty} dk k f(k) J_0(kr) e^{-\alpha t/k^2} . \quad (26)$$

Setting  $t = 0$  in Eq. (26) and using the Fourier-Bessel Theorem, one can derive the following identity for the Fourier-Bessel amplitude

$$f(k) = \int_0^{\infty} dr r \varphi(r, t=0) J_0(kr) . \quad (27)$$

As an example, consider a blob that has an initial Gaussian distribution in radius, i.e.  $\varphi(r, t=0) = \varphi_b \exp[-(r^2/2r_b^2)]$ . Carrying out the integral we find that  $f(k) = \varphi_b r_b^2 \exp[-(k^2 r_b^2/2)]$ , so that for this case the general solution is

$$\varphi_0 \equiv \varphi(r, t) = \varphi_b r_b^2 \int_0^{\infty} dk k e^{-k^2 r_b^2/2} J_0(kr) e^{-\alpha t/k^2} . \quad (28)$$

Note that  $\varphi_0$  and its associated vorticity decay in time due to the parallel current flowing into the plates [the  $\alpha$  term in Eq. (24)].

The decay of  $\varphi_0$  for a Gaussian vorticity blob is illustrated numerically in Fig. 1, where we have plotted  $\varphi_0$  in Eq. (28) vs the normalized radius  $\rho = r/r_b$  for three values of the scaled time,  $\tau = 2\alpha r_b^2 t = 0, 3$  and  $6$ . Figure 1 shows that the radial scale of the potential decreases as time elapses. This illustrates that the decay rate for each Fourier-Bessel component of  $\varphi_0$  is related to its scale length,  $\gamma_\varphi = \alpha/k^2$ , and for a Gaussian blob the decay rate is related to its size,  $\gamma_\varphi \sim \alpha r_b^2$  [see Eq. (28)]. Thus, the potential  $\varphi$  survives the longest in the smallest blobs, whereas the decay of the Bohm potential  $\Phi_B$  is independent of blob size. Finally, note that  $\gamma_\varphi \gg \gamma_n$  when  $r_b \gg 1$ , and the latter inequality is required for fluid theory to be valid. Thus, the potential  $\varphi$  also helps to symmetrize the density blobs.

In summary, there are two sources of blob vorticity which can cause blob azimuthal rotation and symmetrization of its density. There are independent mechanisms for the decay of each source of vorticity: the parallel flow of energy and its transmission through the sheath causes  $\Phi_B$  to decay in time on the temperature time scale  $\tau_T$ , whereas the flow of parallel currents to the sheaths causes  $\varphi$  to decay with a characteristic timescale of  $\tau_\varphi \approx \gamma_\varphi^{-1} = 1/\alpha r_b^2$ . Both of these times are shorter than the density decay time  $\tau_n \approx \tau_T \alpha_T / \alpha \approx 1/\alpha$ , so that our assumption of cylindrically-symmetric density blobs seems justified in the presence of an initial source of vorticity.

### C. Physical Picture and Validity Conditions

The results of the preceding sections can be combined to obtain a unified physical picture of non-interacting, propagating blobs that are created with an initial vorticity, temperature and density higher than the SOL background values. Our calculation has employed an expansion in the small parameter  $1/r_b$  with the vorticity and temperature physics described in order unity [Sec. III B] and the density physics emerging in order

$1/r_b$  [Sec. III A]. In this section, we summarize the resulting physical picture and the validity conditions for our analysis. These conditions make use of the results that the decay times of  $\varphi$ ,  $\Phi_B$  (and  $T$ ), and  $n$  are approximately  $\tau_\varphi \approx 1/\alpha r_b^2$ ,  $\tau_T \approx 1/\alpha_T$ , and  $\tau_n \approx 1/(\alpha - \xi)$ , respectively, where we now re-introduce the effect of ionization ( $\xi = \text{const.} \neq 0$ ) for this heuristic discussion.

As a result of its initial vorticity,  $\nabla_\perp^2(\varphi_0 + \Phi_B)$ , the spinning blob symmetrizes the density,  $n(r, \theta) \rightarrow n(r)$ . For this to occur, the rotational time around its axis (eddy time) must be much less than the vorticity decay time for at least one of the two sources of vorticity, i.e. one of the following conditions must be satisfied:

$$\alpha r_b^4 \ll \varphi_0 \quad , \quad \alpha_T r_b^2 \ll \Phi_B \quad . \quad (29)$$

The validity condition for neglecting the higher order terms ( $\sim \beta$ ) in our solution for the time dependence of  $\varphi_0$  was

$$\beta \ll \alpha^2 r_b^5 \quad . \quad (30)$$

The vorticity (and lowest order potential) decays away faster than the density if both of the following conditions are satisfied:

$$\alpha - \xi \ll \alpha r_b^2 \quad , \quad \alpha - \xi \ll \alpha_T \quad . \quad (31)$$

In the absence of ionization ( $\xi = 0$ ), the inequalities in Eq. (31) reduce to  $1 \ll r_b^2$  and  $1 \ll S_E$ , respectively.

The strong rotation condition, Eq. (29), may not always be satisfied, but it is not essential for the main results of this paper pertaining to density blob transport. For typical parameters, Eq. (31) is always satisfied. When the initial potential has decayed to a sufficiently low value, the vorticity can be neglected in Eq. (9) and the simple density blob solution of Sec. III A is recovered. The condition for this is just the reverse of Eq. (29), viz.

$$\varphi_0 \ll \alpha r_b^4 \quad , \quad \Phi_B \ll \alpha_T r_b^2 \quad . \quad (32)$$

On the slower density time scale, the curvature drift in the y direction polarizes the blob by causing the electrons and ions to move in opposite directions. This charge separation creates a potential  $\varphi(y)$  and electric field  $E_y$ , which in turn result in an  $\mathbf{E} \times \mathbf{B}$  drift of the blob outwards in the x direction with a radial velocity that depends on the blob size,

$$u_x = \frac{\beta}{\alpha} \frac{1}{r_b^2} \quad . \quad (33)$$

To make a significant contribution to the particle transport, the density blobs must propagate a significant distance in x before decaying. The minimum distance the blobs must propagate for the theory to make sense is one blob radius. This ensures that the creation region is separate from the region where one is calculating the transport. If the blobs decay before leaving the creation region, they do not contribute to the transport. The condition that each blob drift outwards a distance much greater than one blob radius  $r_b$  before decaying is

$$r_b \ll \left[ \frac{\beta}{\alpha(\alpha - \xi)} \right]^{1/3} \quad . \quad (34)$$

Note that ionization can sustain the blob longer against the parallel loss of particles and thus allows larger blobs to contribute to transport. The outward propagation of Gaussian blobs of radius  $r_b$  gives SOL density and temperature profiles with radial scale lengths  $L_{nx} = u_x \tau_n$  and  $L_{Tx} = u_x \tau_T$  given by

$$\begin{aligned} L_{nx} &= \frac{\beta}{\alpha(\alpha - \xi)r_b^2} \Rightarrow L_{nx} = \frac{L_{\parallel}^2 / R}{1 - \tau_{\parallel} / \tau_i} \left( \frac{\rho_s}{r_b} \right)^2 , \\ L_{Tx} &= \frac{\beta}{\alpha \alpha_T r_b^2} \Rightarrow L_{Tx} = \frac{L_{\parallel}^2 / R}{S_E} \left( \frac{\rho_s}{r_b} \right)^2 , \end{aligned} \quad (35)$$

where the second form gives the dimensional scaling with  $\tau_{\parallel} = L_{\parallel}/(2c_s)$  and  $\tau_i = 1/(n_n \langle \sigma v \rangle_i)$ . Note that either small blobs ( $r_b \rightarrow 0$ ) or the effects of ionization ( $\alpha - \xi \rightarrow 0$ ) can give flat density scale lengths. However, significant ionization can occur only if the electron temperature exceeds the ionization energy. This requires that the temperature profile be broad enough, viz. that  $L_{T_x}$  be comparable to the SOL width. The self-consistent treatment of ionization in the blob model will be discussed further in Sec. V. Finally, we note that Eqs. (34) and (35) imply that the gradient scale lengths are long compared to the blob size, which is a necessary condition for the theory to make sense.

Taking into account all of these results, the validity conditions for the simple density blob model of Sec. III A can be summarized as

$$\text{Max} \left[ \left( \frac{\beta}{\alpha^2} \right)^{1/5}, \left( \frac{\varphi_0}{\alpha} \right)^{1/4}, \left( \frac{\Phi_B}{\alpha_T} \right)^{1/2}, \left( \frac{\alpha - \xi}{\alpha} \right)^{1/2} \right] \ll r_b \ll \left[ \frac{\beta}{\alpha(\alpha - \xi)} \right]^{1/3}. \quad (36)$$

If Eq. (34) is satisfied, both  $\varphi_0$  and  $\Phi_B$  decay more rapidly than the density and the inequalities in Eq. (36) involving these potentials are automatically satisfied on the slow time scale of the density blobs. For typical parameters ( $\alpha \sim \beta \sim 10^{-4}$ ) and in the absence of ionization ( $\xi = 0$ ), the remaining inequalities imply that the simple density blob theory is valid for  $r_b > 10$  and predicts transport from blobs in the range  $r_b < 50$ , where we recall that  $r_b$  is defined in units of  $\rho_s$ . Larger size blobs can contribute to transport when sustained by ionization ( $\xi \neq 0$ ).

The most interesting feature of the blob model is that the outward velocity and penetration length of a density blob depends on its size. Thus, a quantitative estimate of the SOL density and particle flux can only be obtained by taking an average over the size distribution of the ensemble of blobs. We turn to this question in the next section.

## IV. Blob Ensemble Averaging

### A. Ensemble-Averaged Profiles

We now consider an ensemble of blobs with a size distribution function  $f(r_b)$ , specifying the number of blobs whose radius lies in the range  $dr_b$  centered on  $r_b$ . For simplicity, we assume that all blobs have the same amplitude,  $n_b(r = 0) = n_{b0}$ , independent of their cross-sectional area. The corresponding ensemble average is defined as

$$\langle Q \rangle = \frac{\int_1^{r_{\max}} dr_b r_b f(r_b) Q}{\int_1^{r_{\max}} dr_b r_b f(r_b)} . \quad (37)$$

Here, the lower bound of integration is cut off at the gyroradius ( $r_b = 1$ ). The upper cut-off is determined by the requirement that the blob move fast enough before decaying to contribute to transport, i.e.  $r_{\max} = (\beta/\alpha\gamma_n)^{1/3}$  by Eq. (34). This cut-off can also be derived rigorously by carrying out the transformation from the lab frame to the blob frame of reference and requiring a convergent integral. Since the blobs are formed at or inside the separatrix ( $x = 0$ ) and then propagate across the SOL, we evaluate  $r_{\max}$  at  $x = 0$  and hold it fixed as the blobs propagate through the SOL.

By integrating over the ensemble of blobs, one can obtain expressions for the SOL density profile  $n(x)$ , the outward plasma flux  $\Gamma(x)$ , and other profiles. The size distribution of the blobs is regarded as input to the present theory and could be inferred from either turbulence simulations or experimental data. Although a formal derivation of the density and flux integrals has been carried out, here we give a heuristic one.

We assume that the blobs are created by some turbulent process that is intermittent in both space and time and which ejects the blobs into the SOL. Let  $\tau$  be the ensemble-averaged time between the creation of consecutive blobs. We assume a separation of scales in which blobs created in a small region near the separatrix propagate

radially to the region near the wall which is “far away” compared to the size of even the largest blobs in the system,  $r_{\max} \ll u_x \tau$ .

We define the average density  $n(x)$  and outward plasma flux  $\Gamma(x)$  by

$$n(x) = \langle n_b(x, r_b) \rangle, \quad \Gamma(x) = \langle n_b(x, r_b) u_x(r_b) \rangle, \quad (38)$$

where the ensemble average  $\langle \dots \rangle$  was defined in Eq. (37),  $n_b(x, r_b) = N(x, r_b)/V_b$  denotes the average density of particles in a single blob of radius  $r_b$  centered at position  $x$ ,  $N(x, r_b)$  is the total number of particles in the blob, and  $V_b = r_b L_{\parallel} u_x \tau$  is the effective volume swept out by the blob during the time  $\tau$ . The quantity  $N$  is calculated in terms of the “local” Gaussian blob density profile of Sec. III A,  $n(r) = n_{b0} \exp[-(r^2/2r_b^2)]$ , as follows

$$\begin{aligned} N(x, r_b) &= 2\pi L_{\parallel} \int_0^{\infty} dr r n_{b0} e^{-r^2/2r_b^2} e^{-\gamma x/u_x}, \\ &= 2\pi L_{\parallel} n_{b0} r_b^2 e^{-\gamma x/u_x}, \end{aligned} \quad (39)$$

where  $u_x = \beta/(\alpha r_b^2)$  and the assumed separation of scales allows us to extend the limit of integration in  $r$  to infinity. The exponential factor takes into account the parallel decay of the particles (assuming that the blobs leave the separatrix  $x = 0$  at  $t = 0$  so that they pass the position  $x$  at time  $t = x/u_x$ ) and uses the notation  $\gamma = \gamma_n = \alpha - \xi$ . Combining all of these definitions and carrying out the integrals gives the following results for the density and flux profiles:

$$n(x) = \frac{2\pi n_{b0} \alpha}{\tau \beta} \frac{\int_1^{r_{\max}} dr_b r_b^4 f(r_b) e^{-\mu x r_b^2}}{\int_1^{r_{\max}} dr_b r_b f(r_b)}, \quad (40)$$

$$\Gamma(x) = \frac{2\pi n_{b0}}{\tau} \frac{\int_1^{r_{\max}} dr_b r_b^2 f(r_b) e^{-\mu x r_b^2}}{\int_1^{r_{\max}} dr_b r_b f(r_b)}, \quad (41)$$

where  $\mu = \alpha\gamma/\beta$ . The expressions in Eqs. (40) and (41) were also obtained rigorously by carrying out the formal transformation from the lab frame to the blob frame of reference and defining appropriate spatial and time averages. Note that the exponent of  $r_b$  in the density and flux integrals differ by a factor of 2 because of the form of  $u_x$  in Eq. (33).

## B. Power-Law Distributions

Given the ubiquitous occurrence of power law distributions in simulations of turbulence and in Self-Organized Criticality (SOC) models,<sup>19,20</sup> it is interesting to evaluate the ensemble-averaged density and flux profiles in Eqs. (40) and (41) using a power law distribution of blob radii,

$$f(r_b) = \frac{1}{r_b^p} . \quad (42)$$

The density and flux profiles are then given by

$$n(x) = \frac{2\pi n_{b0}}{\tau} \frac{\alpha}{\beta} \frac{\int_1^{r_{\max}} dr_b r_b^{4-p} e^{-\mu x r_b^2}}{\int_1^{r_{\max}} dr_b r_b^{1-p}} , \quad (43)$$

$$\Gamma(x) = \frac{2\pi n_{b0}}{\tau} \frac{\int_1^{r_{\max}} dr_b r_b^{2-p} e^{-\mu x r_b^2}}{\int_1^{r_{\max}} dr_b r_b^{1-p}} .$$

Similarly, one can derive an ensemble-averaged radial scale length  $L_x(x)$  and an “effective diffusion coefficient”  $D_{\text{eff}}(x)$ , which are given by

$$L_x(x) \equiv \frac{-n(x)}{dn/dx} = \frac{1}{\mu} \frac{\int_1^{r_{\max}} dr_b r_b^{4-p} e^{-\mu x r_b^2}}{\int_1^{r_{\max}} dr_b r_b^{6-p} e^{-\mu x r_b^2}} \quad (44)$$

$$D_{\text{eff}}(x) \equiv \frac{-\Gamma(x)}{dn/dx} = \frac{\beta}{\alpha\mu} \frac{\int_1^{r_{\text{max}}} dr_b r_b^{2-p} e^{-\mu x r_b^2}}{\int_1^{r_{\text{max}}} dr_b r_b^{6-p} e^{-\mu x r_b^2}}$$

Finally, note that these definitions yield the following expressions involving the ensemble-averaged radial velocity  $u_x(x)$ :

$$u_x(x) = \frac{\Gamma(x)}{n(x)} = \frac{D_{\text{eff}}(x)}{L_x(x)}, \quad (45)$$

which serves as a check on the self-consistency of our definitions.

Sample density and flux profiles are shown in Fig. 2, where we plot the normalized profiles  $n(x_n)/n(0)$  and  $\Gamma(x_n)/\Gamma(0)$  vs  $x_n = x/r_{\text{max}}$  for  $p = 1$  and  $p = 4$ . This plot corresponds to the parameters  $B = 30$  kG,  $T_e = 50$  eV,  $R = 100$  cm,  $L_{\parallel} = 4\pi R$ , which imply  $\alpha = 0.5 \times 10^{-4}$  and  $\beta = 6.8 \times 10^{-4}$ . In this figure we consider the case without ionization ( $\xi = 0$ ) in order to emphasize the effect of blob size on the profiles. For  $p = 1$  the large slow blobs dominate the transport. They do not penetrate very far before decaying due to parallel particle flow to the sheaths, yielding exponentially decaying profiles. For  $p = 4$  the small fast blobs dominate the transport. Since the small blobs move faster, they can travel much farther before decaying and therefore produce flatter density and flux profiles, consistent with the estimate given in Eq. (35) from the single blob model. Also note that the flux profile flattens faster (as a function of  $p$ ) than the density profile, because it is weighted by the radial velocity. The boundary  $p = p_{\text{crit}}$  between the two regimes illustrated in Fig. 2 can be estimated analytically for the power-law distribution of blob radii, as discussed in Appendix B.

The behavior in Fig. 2 is consistent with recent measurements on the Alcator C-Mod tokamak.<sup>21</sup> As discussed in Sec. I, C-Mod has observed flattened density profiles and large recycling near the wall in their ‘‘Main Chamber Recycling Regime’’.<sup>1,2</sup> If one attempts to interpret such profiles in terms of a diffusive model, the effective diffusion

coefficient increases with  $x$  and becomes large near the wall. *This behavior arises naturally in the blob model.* The small fast blobs penetrate farther into the SOL than the large slow blobs, so that the ensemble-averaged  $u_x(x)$  increases with distance into the SOL and the density profile flattens [ $L_x(x)$  increases], even in the absence of ionization and recycling. But Eq. (45) implies that  $D_{\text{eff}}(x) = u_x(x) L_x(x)$  so that the effective diffusion coefficient increases very rapidly with  $x$  in the blob model. This behavior is a simple consequence of the size-dependent velocity in Eq. (33). In the strong recycling regime, the ionization source also helps to broaden the density profile, as discussed in Sec. V.

## V. Role of Ionization

There are two radial regions in the SOL in which ionization plays different roles: (1) near the separatrix the density profile is dominated by the balance of perpendicular transport with parallel flows; it decays exponentially because typically ionization of neutrals is not sufficient to compensate for the parallel losses ( $\xi \ll \alpha$ ); (2) near the wall the neutral density is larger than the plasma density and the plasma density profile is dominated by recycling and ionization, which can balance the parallel outflow of particles and lead to relatively flat density profiles.

While not specific to blob theory, this picture of the outer SOL is enhanced when blobs are present. In Sec. III C we showed that ionization can enhance the SOL penetration of the density blobs and significantly increase  $L_{nx}$ . Since the source of neutrals is recycling at the wall, there is a *synergy between blob propagation and recycling*. The fast radial propagation of the small blobs flattens the density profile and increases the plasma density at the wall. This plasma flux to the wall in turn increases the recycling of neutrals, which increases the ionization source that sustains the blob transport.

To illustrate these points, we examine the equilibrium conditions at the wall, located at  $x = x_w$ , using a simple model. We assume that there is a region near the wall of width  $\Delta x = x_w - x_0$  in which both the plasma and neutral density profiles are flat. Here,  $x_0$  denotes the starting point of this interval in which the profiles are flat. The assumption of constant density requires  $\Delta x \ll \lambda_{0w} = (v_0/v_0)_w$  for self-consistency, where  $\lambda_0$  is the neutral mean free path,  $v_0$  is the neutral thermal velocity,  $v_0 = n\langle\sigma v\rangle_i$  is the ion-neutral ionization frequency,  $\langle\sigma v\rangle_i$  is the ionization rate, and the subscript  $w$  implies that the quantity is evaluated at the wall. For simplicity, we assume that the electron temperature  $T$  and ionization rate  $\langle\sigma v\rangle_i$  are also constant in this narrow neutral layer and neglect the temperature equation. This is consistent if  $\Delta x \ll L_{Tx}$  [defined in Eq. (35)]. In order for ionization to occur, the electron temperature in this layer must exceed the ionization energy cost,  $T_w > E_i$ .

The steady state condition ( $\gamma = 0$ ) that ionization balance the parallel flows in the region near the wall is

$$\alpha = \xi_w \equiv n_{0w} S \quad , \quad (46)$$

where  $S = \langle\sigma v\rangle_i/(\rho_s^2 c_s)$  is the dimensionless ionization rate. The neutral density at the wall is given by the recycling condition

$$n_{0w} v_0 = R_c \Gamma(x_w) \quad , \quad (47)$$

where  $R_c$  is the recycling coefficient. Combining these two equations gives the equilibrium condition

$$\Gamma(x_w) = \frac{\alpha v_0}{R_c S} \quad . \quad (48)$$

The equilibrium condition (48) places a constraint on the existence of the equilibrium solution. Since the ionization rate  $S(T)$  is a strong function of electron temperature, Eq. (48) determines the plasma flux to the wall,  $\Gamma_w = \Gamma(x_w)$ , required to sustain the

equilibrium for a given electron temperature  $T$  (or vice versa). For a given neutral species, the ionization rate  $S(T)$  is non-monotonic, becoming small for both  $T \rightarrow 0$  and  $T \rightarrow \infty$  and having a maximum value  $S_{\max}$  for some intermediate electron temperature. Thus, there is a minimum required flux,  $\Gamma_{w,\min}$ , for Eq. (48) to have a solution. For  $\Gamma_w < \Gamma_{w,\min}$ , an equilibrium solution does not exist and the plasma density will decay near the wall. The existence of a critical cross-field plasma flux to maintain the “Main Chamber Recycling Regime” was also noted in Ref. 2.

This analysis illustrates the important result that if the flux  $\Gamma_w$  and temperature  $T_w$  in the far SOL exceed certain thresholds, one can obtain constant plasma density, neutral density and flux profiles from the blob model in the region near the wall. The density  $n_w$  and flux  $\Gamma_w$  are obtained by evaluating the integrals in Eqs. (40) and (41) with  $\gamma = 0$ , and the neutral density  $n_{0w} = n_0(x_w)$  is obtained from the recycling condition, Eq. (47). The temperature  $T_w$  can be estimated from an integral analogous to Eq. (40) in which  $n_{b0} \rightarrow T_{b0}$  and  $\gamma \rightarrow \gamma_T \neq 0$ . A realistic treatment would take into account the spatial variation of  $n(x)$ ,  $n_0(x)$  and  $T(x)$  (and hence  $\langle \sigma v \rangle_i$ ) across the SOL by a numerical solution of the coupled plasma density, neutral density and electron temperature equations, but would yield the same basic physics.

## VI. Summary and Discussion

In this paper, we have examined the theory of non-interacting blobs in the absence of a background plasma (appropriate to the far SOL region) based on a simple three-field fluid model described in Sec. II. The blobs were treated as coherent propagating structures with local concentrations of density, temperature and vorticity. The physics of single blobs was investigated in Sec. III. It was shown that the vorticity symmetrizes the density and decays away before propagating a significant distance. The blob temperature also decays faster than its density, because parallel energy transport is faster than parallel particle transport. Also, ionization can partly counteract the parallel loss of particles, but

enhances the decay of the temperature. The density blobs convect plasma to the wall due to a charge separation driven by the curvature drift (in toroidal devices) or the centrifugal force (in rotating linear machines). This charge separation gives rise to an electrostatic potential  $\phi(y)$  and electric field  $E_y$  which causes an outward drift  $u_x$ . The most important feature of the blob model is that  $u_x$  is inversely proportional to the area of the blob ( $\propto r_b^2$ ), so that smaller blobs propagate faster than larger ones. This sensitivity to the blob size requires that the average SOL profiles be defined in terms of an ensemble average over a blob size distribution function, as discussed in Sec. IV.

The present analysis suggests that the propagation of density blobs<sup>17</sup> is a possible explanation for the non-diffusive, intermittent SOL transport observed in many fusion experiments. Even the simple model used here has several properties (inherent to blob physics) that are in qualitative agreement with data for the “far SOL” in various experiments. These properties can be summarized as follows:

- (1) the local density, temperature and vorticity are intermittent in space and time (i.e.  $\delta n/n \sim 1$ );
- (2) the temperature and vorticity of the blobs decay in time faster than the density;
- (3) the radial transport of particles is convective, and the average radial velocity and effective diffusion coefficient increase towards the wall;
- (4) the average blob size decreases towards the wall;
- (5) the density and particle flux at the wall is finite, and the profiles are flat in some regimes;
- (6) the SOL equilibrium depends on wall recycling and ionization, and there is a minimum plasma flux to the wall required to sustain the equilibrium.

In regard to the last point, we have noted in Sec. V that there is a *synergy between the blob propagation and the recycling*: the blobs increase the plasma flux to the wall, which increases the recycling; the recycling in turn increases the ionization that helps fuel the

blob particle transport to the wall. This reasoning suggests that neutral density should be an important parameter controlling the blob transport.

As a first attempt at a more quantitative theory, in Sec. IV B we considered power law blob-size distributions,  $f(r_b) = 1/r_b^p$ . We found that the large blobs dominate the density and flux profiles for  $p < p_{\text{crit}}$  and the small blobs dominate for  $p > p_{\text{crit}}$ , where  $p_{\text{crit}} = 2$  for  $\gamma_n \neq 0$  in our normalization of the ensemble average, Eq. (37) [see Appendix B]. The SOL profiles are significantly flatter in the large- $p$  limit because of the higher velocity of the smaller blobs. It would be interesting to do a statistical analysis of the results of experimental data and turbulence simulations to obtain the relevant power law distributions for the observed blobs.

A detailed discussion of experimental data is beyond the scope of this paper, but it should be pointed out that recent statistical analyses of turbulence data have some points of contact with the present model. SOL diagnostics on several experiments have measured statistically-rare large-amplitude events with long correlation times that are consistent with the existence of large-scale, spatially-coherent, radially-propagating structures.<sup>13,22,23</sup> This behavior tends to be more pronounced in the far SOL region and at high plasma density. The propagating structures can be responsible for a significant fraction of the inferred radial particle and energy transport in the far SOL.<sup>13,22,23</sup>

In the main body of the paper, some approximations were made which should be generalized for comparison with experiments. First, motion in the  $y$  direction was neglected by treating the temperature as spatially constant. Extension of the theory to include a sheared velocity component  $u_y(x)$  and temperature gradient  $T(x)$  is discussed in Appendix A, where it is shown that a sheared  $u_y(x)$  distorts the blob shape, but does not affect the radial velocity  $u_x$  if  $T$  is constant in  $x$ . The constant- $T$  approximation may be appropriate for the far SOL in the large convection limit. When  $T$  decreases with  $x$ , propagation to a cooler region can reduce  $u_x$  and cause the blob to stretch in the  $y$  direction. It is also noted in Appendix A that geometric effects could affect the radial

velocity of blobs having large poloidal extent. Finally, in the present theory the density blob velocity  $u_x$  depends on its spatial extent  $r_b$  but is independent of its amplitude  $n_b$ . This may be related to our neglect of a background density. One might expect nonlinear coupling of the blob to the background to affect its velocity of propagation across the SOL and introduce a dependence on  $n_b$ . These effects should be included in a quantitative theory, but are outside the scope of the present paper.

More generally, the present work has not investigated the physics of blob creation, nor the explicit connection between the blobs and the saturated coherent structures observed in turbulence simulations and data. It is hoped that the results of this paper will motivate such studies and provide a framework for the analysis of experimental data.

## Acknowledgements

This work was supported by the U.S. Department of Energy (DOE) under DOE Grants No. DE-FG03-97ER54392 and DE-FG03-00ER54568; however, this support does not constitute an endorsement by the DOE of the views expressed herein.

## Appendix A

In this Appendix, we generalize the discussion in the main body of the paper to include a background temperature gradient  $T(x)$  and a sheared poloidal blob velocity,  $v_y(x)$ , as is sometimes observed in the experiments and simulations. An important question relevant to the radial transport is whether these physical effects modify the radial blob velocity  $v_x$ . The notation in this Appendix is slightly modified from the main text: here, we use the dimensional form of the equations and  $\mathbf{v}$  denotes the blob velocity.

We employ the following ansatz for the blob velocity

$$v_x = \text{constant in space and time}, \quad (\text{A1})$$

$$v_y = v_0(x, t) . \quad (\text{A2})$$

Here  $v_0$  denotes the total y velocity, including both a driven velocity component (e.g. due to biasing of divertor end plates) and the self-consistent response of the blob to the imposed flow, which is calculated below. Using the fact that  $\mathbf{E} \times \mathbf{B}$  drifts give incompressible flow ( $\nabla \cdot \mathbf{v} \approx 0$  neglecting the small curvature term) and working to lowest order in  $1/r_b$ , the density equation becomes

$$\frac{dn}{dt} = \frac{\partial n}{\partial t} + v_x \frac{\partial n}{\partial x} + v_y(x, t) \frac{\partial n}{\partial y} = 0 . \quad (\text{A3})$$

The solution to this equation is  $n = n(x', y')$ , where  $x'$  and  $y'$  are the constants of motion obtained by solving the trajectory equations in the primed frame of reference

$$\frac{dx'}{dt'} = v_x' , \quad (\text{A4})$$

$$\frac{dy'}{dt'} = v_y' = v_0(x', t') , \quad (\text{A5})$$

subject to the initial conditions

$$x'(t' = t) = x, \quad y'(t' = t) = y . \quad (\text{A6})$$

Setting  $t' = 0$  without loss of generality, the solution to these equations is given by

$$x' = x - v_x t , \quad (\text{A7})$$

$$y' = y + \eta(x, t), \quad \eta(x, t) = - \int_0^t dt'' v_0(x, t'') . \quad (\text{A8})$$

This solution is valid for any function  $v_0(x, t)$  and any choice of  $n(x', y')$ .

The Gaussian density blob solution of Sec. III A2 is recovered by choosing

$$n = n_b \exp\left(-\frac{x'^2 + y'^2}{2r_b^2}\right) , \quad (\text{A9})$$

and the potential  $\phi$  arising from the curvature-drift polarization of the blob [see Eq. (11)] is given by

$$\frac{e\phi}{T} \equiv \frac{L_{\parallel}\rho_s}{R} \frac{\partial \ln n}{\partial y} . \quad (\text{A10})$$

Substituting Eq.(A9) into Eq. (A10), one obtains

$$\frac{e\phi}{T} = -\frac{L_{\parallel}\rho_s}{Rr_b^2} y' = -\frac{L_{\parallel}\rho_s}{Rr_b^2} [y + \eta(x,t)] , \quad (\text{A11})$$

and using Eqs. (A2) and (A11) we obtain the final form of the blob  $\mathbf{E} \times \mathbf{B}$  drift velocity:

$$v_x = -\frac{c}{B} \frac{\partial \phi}{\partial y} = c_s \frac{L_{\parallel}\rho_s^2}{Rr_b^2} \quad (\text{A12})$$

$$\begin{aligned} v_y \equiv v_0(x,t) &= w(x) + \frac{c}{B} \frac{\partial \phi}{\partial x} , \\ &= w - \frac{\partial [v_x \eta(x,t)]}{\partial x} , \end{aligned} \quad (\text{A13})$$

where  $w(x) = v_y(t=0)$  is the imposed  $y$  velocity and the second term in Eq. (A13) is the self-consistent response. Finally, note that Eq. (A9) implies that the centroid  $(x_c, y_c)$  of the blob (point of maximum density) is given by  $x' = 0 = y'$ , and Eqs. (A7) - (A8) imply that  $x_c = v_x t$ ,  $y_c = -\eta(x,t)$ .

The general solution in Eqs. (A7) – (A13) has the following important property for any choice of  $v_0(x,t)$ . The assumption of spatially constant  $v_x$  in Eq. (A1) requires constant temperature, because Eq. (A12) implies that  $v_x \propto T^{3/2}$ . Thus, when  $T$  is independent of  $x$ , constant  $v_x$  is compatible with a sheared  $v_y(x)$ . This means that the poloidal velocity shear by itself cannot affect the radial velocity of the blobs, although it can greatly distort their shape. Experimental data suggests that  $T$  independent of  $x$  may be a good approximation in the far SOL where the blob transport dominates.

To illustrate another property of this solution, we consider the particular case

$$v_0(x,t) = u(t) e^{-x/L} , \quad (\text{A14})$$

so that Eqs. (A8) and (A13) give

$$\eta(x,t) = w t e^{-v_x t/L}, \quad u(t) = -w \left(1 - \frac{v_x t}{L}\right). \quad (\text{A15})$$

The centroid position is then given by

$$x_c(t) = v_x t, \quad y_c(t) = -w t e^{-v_x t/L}. \quad (\text{A16})$$

Equation (A16) shows that the center of the blob moves with a constant  $v_x$  but its velocity in the  $y$  direction changes sign for large  $t$ . The centroid position  $y_c$  starts out at zero, moves down and then returns to zero as  $t \rightarrow \infty$ . A corresponding plot of the entire blob shows that the blob elongates and distorts diagonally for small  $t$ , but returns to its initial circular shape at large  $t$ . What is depicted by this solution is that the blob eventually propagates in  $x$  to a region where the imposed  $v_y$  and its shear are negligible compared to the flow from the self-consistent potential, which acts to restore the blob to its cylindrically symmetric form. This example illustrates that the type of complicated behavior observed in some simulations (e.g. blobs moving back and forth) can be recovered from this simple extension of our blob model.

For completeness, we should mention that there are two situations in which  $v_x$  may change as the blob propagates across the SOL. A perturbative calculation with  $T(x) = (1 - x/L \dots)$ , where  $x/L$  is assumed small, suggests that the blobs slow down because  $v_x \propto T^{3/2}$  and that they elongate in the  $y$  direction. The latter result comes from Eqs. (A8) and (A13), since  $v_x = v_x(x)$  gives a term in  $v_y = -y \partial_x v_x(x)$  with  $\partial_x = \partial/\partial x$ . Thus, a temperature gradient can modify the radial blob velocity, but this is likely to be a small effect in the far SOL. For blobs that have a large poloidal extent, another effect comes into play, viz. that the effective curvature driving the radial motion must be averaged poloidally and may vary radially, especially if the rotational transform is a strong

function of  $x$  due to the presence of an X-point. These effects are outside the scope of the present paper.

## Appendix B

Here, we derive an analytic condition for the boundary between the two transport regimes illustrated in Fig. 2 for the power-law blob size distribution  $f(r_b) = 1/r_b^p$ . It was shown in Fig. 2 that the main contributors to the particle transport depend on the power law exponent  $p$ : the transport is dominated by the large blobs for small  $p$  (yielding exponentially-decaying density and flux profiles) and by the small blobs for large  $p$  (giving flatter profiles).

The critical exponent  $p = p_{\text{crit}}$  separating these two regimes can be determined by investigating the properties of the integrals in Eq. (43). The technique we use to determine  $p_{\text{crit}}$  is to calculate the functions  $n(p)$  and  $\Gamma(p)$  in the limit  $r_{\text{max}} \rightarrow \infty$ . If the large blobs dominate one of the integrals in Eq. (43), this integral will diverge in the limit  $r_{\text{max}} \rightarrow \infty$ , yielding a value of  $n$  or  $\Gamma$  that is either infinite or zero, depending on whether the singular integral is in the numerator or denominator. The largest value of  $p$  for which this behavior occurs is defined to be  $p_{\text{crit}}$ . On the other hand, if the integrals are all finite and non-zero as  $r_{\text{max}} \rightarrow \infty$ , we conclude that the small blobs gave the dominant contribution.

The results of these calculations are summarized in Table 1 for the cases  $\gamma = 0$  and  $\gamma \neq 0$ . For  $\gamma = 0$ , the integrals in the numerator and denominator of Eq. (43) yield simple polynomials in  $r_{\text{max}}$ . In the limit  $r_{\text{max}} \rightarrow \infty$ , this analytic result predicts an infinite density for  $p \leq 5$  and an infinite flux for  $p \leq 3$ . The upper bound in each case is defined as the value of  $p_{\text{crit}}$  for the corresponding physical quantity, as shown in Table I. The large blobs dominate these integrals for  $p \leq p_{\text{crit}}$  and should do so also in the more relevant physical limit where  $r_{\text{max}}$  is finite. For  $\gamma = 0$  and  $p > p_{\text{crit}}$ , the density and flux are finite

as  $r_{\max} \rightarrow \infty$ , and we conclude that the small blobs dominate the integrals (for all values of  $r_{\max}$ ).

When  $\gamma \neq 0$ , the integrals in the numerators of the density and flux can be expressed in terms of Exponential Integrals as  $r_{\max} \rightarrow \infty$  and are always finite. The denominator is again a polynomial which diverges as  $r_{\max} \rightarrow \infty$  for  $p \leq 2$  implying that the large blobs dominate the integral. In this limit the analytic result yields a vanishing density and radial flux. The absence of radial flux is consistent with the inequality given in Eq. (34). For  $\gamma \neq 0$ , the limit  $r_{\max} \rightarrow \infty$  violates Eq. (34). The physical interpretation is that the large blobs do not have time to move radially before decaying, and thus their (dominant) contribution to the flux vanishes. For  $\gamma \neq 0$  and  $p > 2$ , the smallest blobs dominate the SOL transport, yielding a finite density and flux.

This analytic result may be of some guidance in interpreting experimental data or the results of turbulence simulations. It also makes a qualitative prediction. Comparing the two cases in Table I suggests that the large-blob transport regime can be extended by ionization (i.e.  $p_{\text{crit}}$  can be increased by decreasing the parallel loss rate  $\gamma$ ).

## Reference

- <sup>1</sup> M. Umansky, S. I. Krasheninnikov, B. LaBombard and J. L. Terry, *Phys. Plasmas* **5**, 3373 (1998).
- <sup>2</sup> B. LaBombard, M. V. Umansky, R. L. Boivin, J. A. Goetz, J. Hughes, B. Lipschultz, D. Mossessian, C. S. Pitcher, J. L. Terry, Alcator Group, *Nucl. Fusion* **40**, 2041 (2000).
- <sup>3</sup> R. Schneider, private communication (2001).
- <sup>4</sup> R. Schneider, D. P. Coster, A. Kallenbach, *et al.*, in *Proceedings of the 17<sup>th</sup> International Conference on Plasma Physics and Controlled Fusion Research*, 1998, (IAEA, Vienna, 1999), paper F1-CN-69/THP2/05.
- <sup>5</sup> G. Y. Antar, P. Devynck, X. Garbet, and S. C. Luckhardt, *Phys. Plasmas* **8**, 1612 (2001).
- <sup>6</sup> G. Y. Antar, S. I. Krasheninnikov, P. Devynck, R. P. Doerner, E. M. Hollmann, J. A. Boedo, S. C. Luckhardt and R. W. Conn, *Phys. Rev. Letters* **87**, 065001 (2001).
- <sup>7</sup> J. F. Drake, P. N. Guzdar, and A. B. Hassam, *Phys. Rev. Lett.* **61**, 2205 (1988).
- <sup>8</sup> B. N. Rogers, W. Dorland, and M. Kotschenreuther, *Phys. Rev. Lett.* **85**, 5336 (2000).
- <sup>9</sup> X. Xu, private communication (2001).
- <sup>10</sup> S. J. Zweben, *Phys. Fluids* **28**, 974 (1985).
- <sup>11</sup> M. Endler, H. Niedermeyer, L. Giannone, E. Holzhauser, A. Rudyj, G. Theimer, N. Tsois and ASDEX team, *Nucl. Fusion* **35**, 1307 (1995).
- <sup>12</sup> R. A. Moyer, R. D. Lehmer, T. E. Evans, R. W. Conn, and L. Schmitz, *Plasma Phys. Contr. Fusion* **38**, 1273 (1996).
- <sup>13</sup> J. Boedo, D. Rudakov, R. Moyer, S. Krasheninnikov, G. Tynan, S. Allen, P. Stangeby, P. West, D. Whyte, “Transport by Intermittent Convection in the boundary of DIII-D”, to appear in *Phys. Plasmas* (2001).
- <sup>14</sup> S. Zweben, R. Maqueda, J. Terry, B. LaBombard, C. S. Pitcher, M. Greenwald, B. Rogers, and W. Davis, *Bull. APS* **45**, 188 (2000).
- <sup>15</sup> R. Maqueda, G. A. Wurden, S. Zweben, L. Roquemore, H. Kugel, D. Johnson, S. Kaye, S. Sabbagh, and R. Maingi, *Rev. Sci. Instr.* **72**, 931 (2001).
- <sup>16</sup> J. L. Terry, B. LaBombard, C. S. Pitcher, M. J. Greenwald, and S. Zweben, *Bull. APS* **45**, 320 (2000).
- <sup>17</sup> S. I. Krasheninnikov, *Phys. Lett. A*, **283**, 368 (2001).
- <sup>18</sup> A. V. Nedospasov, V. G. Petrov, and G. N. Fidel'man, *Nucl. Fusion* **25**, 21 (1985).
- <sup>19</sup> P. H. Diamond and T. S. Hahm, *Phys. Plasmas* **2**, 3640 (1995).
- <sup>20</sup> D. E. Newman, B. A. Carreras, P. H. Diamond, and T. S. Hahm, *Phys. Plasmas* **3**, 1858 (1996).
- <sup>21</sup> I. H. Hutchinson, R. Boivin, F. Bombarda, *et al.*, *Phys. Plasmas* **1**, 1511 (1994).
- <sup>22</sup> B. LaBombard, R. L. Boivin, M. Greenwald, *et al.*, *Phys. Plasmas* **8**, 2107 (2001).
- <sup>23</sup> B. A. Carreras, V. E. Lynch, and B. LaBombard, *Phys. Plasmas* **8**, 3702 (2001).

Table 1 Critical exponents for discriminating the two regimes of density and flux  
 (large blobs dominate for  $p \leq p_{\text{crit}}$ , small blobs for  $p > p_{\text{crit}}$ )

Case	Physical Quantity	$p_{\text{crit}}$
$\gamma = 0$	n	5
	$\Gamma$	3
$\gamma \neq 0$	n	2
	$\Gamma$	2

## Figure Captions

Fig. 1  $\varphi_0(\rho)$  for  $\tau = 0, 3$  and  $6$  [from Eq. (28)], where  $\rho = r/r_b$  and  $\tau = 2\alpha r_b^2 t$ .

Fig. 2 Density (solid line) and flux (dashed line) profiles vs  $x_n = x/r_{\max}$  for (a)  $p = 1$  and (b)  $p = 4$  in the absence of ionization ( $\xi = 0$ )

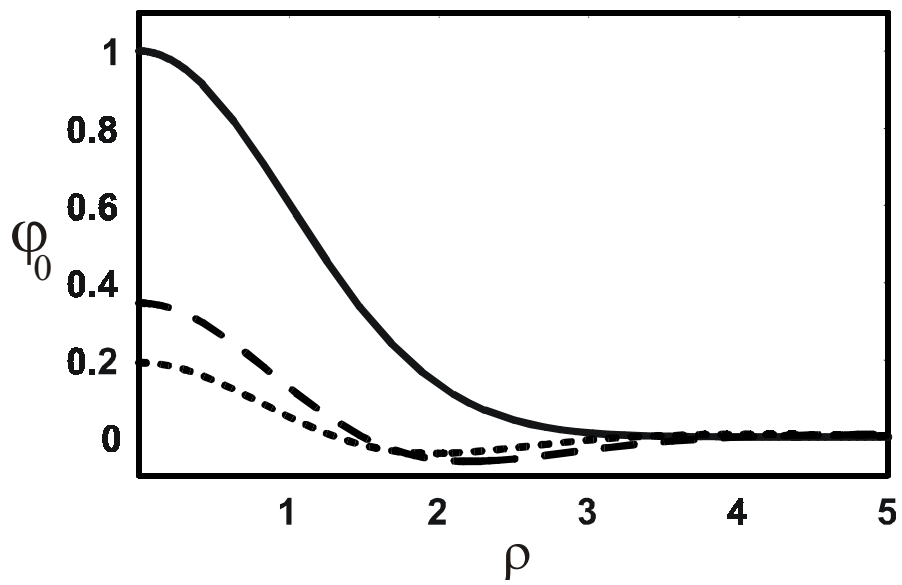


Fig. 1  $\phi_0(\rho)$  for  $\tau = 0, 3$  and  $6$  [from Eq. (28)], where  $\rho = r/r_b$  and  $\tau = 2\alpha r_b^2 t$ .

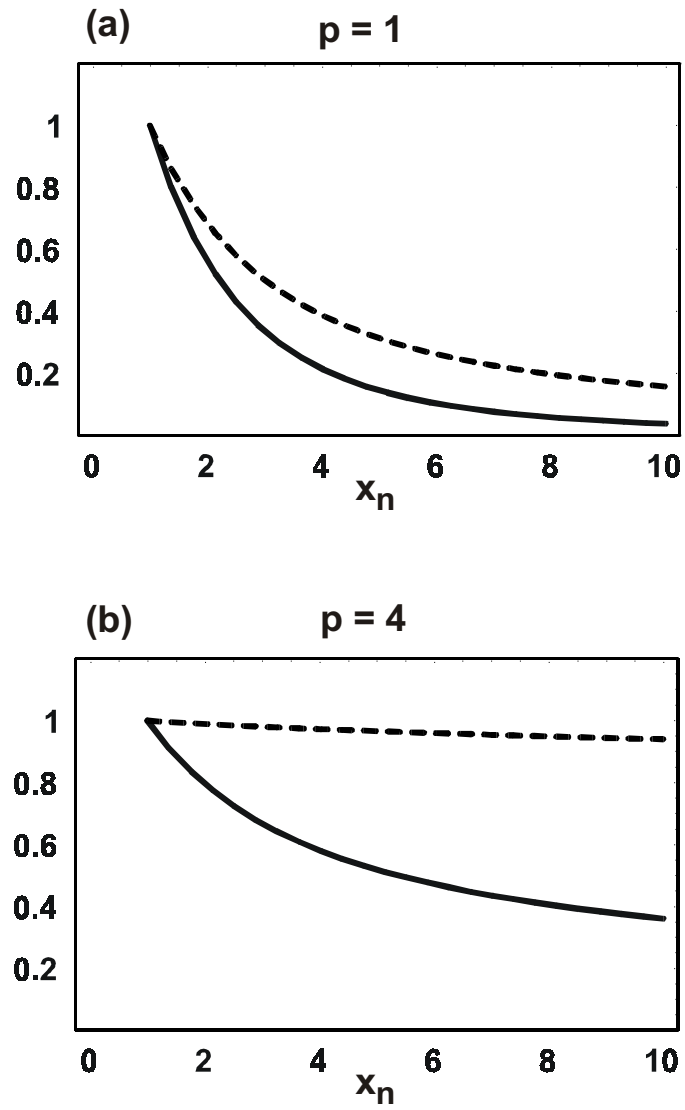


Fig. 2 Density (solid line) and flux (dashed line) profiles vs  $x_n = x/r_{\max}$  for (a)  $p = 1$  and (b)  $p = 4$  in the absence of ionization ( $\xi = 0$ )